Application of Complementary Experimental Techniques to Characterization of the Phase Behavior of $[C_{16}mim][PF_6]$ and $[C_{14}mim][PF_6]$

John De Roche,[†] Charles M. Gordon,*[,‡,#] Corrie T. Imrie,[†] Malcolm D. Ingram,[†] Alan R. Kennedy,[‡] Fabrizio Lo Celso,[§] and Alessandro Triolo*[,||]

Department of Chemistry, University of Aberdeen, Meston Walk, Old Aberdeen AB24 3UE, Scotland, UK, Department of Pure & Applied Chemistry, University of Strathclyde, 295 Cathedral Street, Glasgow G1 1XL, Scotland, UK, Dipartimento di Chimica Physica, Università di Palermo, Viale delle Scienze, Parco D'Orleans 2, I-90128 Palermo, Italy, and Istituto Processi Chimico-Fisici, Sezione di Messina − CNR, Via La Farina 237, 98123 Messina, Italy

Received December 10, 2002. Revised Manuscript Received March 31, 2003

A range of analytical techniques (DSC, conductivity measurement, Raman spectroscopy, small- and wide-angle X-ray diffraction (S-WAXS), quasi-elastic neutron scattering (QENS), and single-crystal X-ray diffraction) are applied to the characterization of the phase behavior of the low-melting-point liquid crystalline salts 1-hexadecyl-3-methylimidazolium hexafluorophosphate ($[C_{16}mim][PF_6]$) and 1-methyl-3-tetradecylimidazolium hexafluorophosphate $[C_{14}mim][PF_6]$. This is the first time that QENS has been applied to the structural analysis of this type of ionic liquid crystal. For the first time in this class of salts, a low-temperature phase transition is identified, which is assigned to a crystal−crystal transition. Conductivity and QENS data for $[C_{16}mim][PF_6]$ suggest that the higher-temperature crystalline phase (C_{II}) has greatly increased freedom in its long alkyl chain and anion than the lower-temperature crystalline phase (C_I). This conclusion is supported by single-crystal X-ray diffraction results for $[C_{14}mim][PF_6]$. In both crystalline phases, as well as in the higher-temperature mesophase, the structure maintains a monodispersed layer structure with interdigitated alkyl chains. The structure of the mesophase is confirmed as smectic A by the S-WAXS and Raman spectroscopy results. Detailed analysis suggests that in this phase the alkyl chains undergo complete conformational melting.

Introduction

Ionic liquid (IL) is the term now widely applied to salts that are liquid at or below 100 °C. ILs show great promise as environmentally benign reaction media for many types of chemical processes.[1] The key to sustainable technology is achieving an economic benefit with environmental improvements: the use of ILs offers improved performances and greater flexibility for a variety of processes such as biphasic catalysis and organic synthesis,[2] separations,[3] electrochemistry,[4] photochemistry,[5] and liquid crystals,[6] potentially leading to economic advantages. ILs are also environmentally benign because they have no detectable vapor pressure, and they promise to make synthetic processes more efficient, thus lowering usage of raw materials. They were first discovered in 1914,[7] but their use as reaction media and catalysts for organic reactions was limited until the mid-1980s. Since that time the number of ILs and of their possible applications has progressively increased. Although many potential applications have been presented, those involving biphasic catalysis are arguably closest to finding industrial applications. To optimize the practical performances of this class of neoteric materials, detailed knowledge of their physical chemical properties is required and, accordingly, a great deal of research activity is in progress to rationalize the behavior of the large number of known ILs.

In this paper we present the results of a study on the solid- and liquid-phase dynamics of 1-hexadecyl-3-methylimidazolium hexafluorophosphate ($[C_{16}mim][PF_6]$) and its tetradecyl analogue $[C_{14}mim][PF_6]$. These salts have been shown previously to display liquid

* Authors to whom correspondence should be addressed via e-mail: C.M.G., gordon@itmc.rwth-aachen.de; or A.T., triolo@me.cnr.it.
[†] University of Aberdeen.
[‡] University of Strathclyde.
[§] Universita di Palermo.
[||] Istituto Processi Chimico-Fisici, Sezione di Messina − CNR.
[#] Current address: RWTH Aachen, Institute for Technical and Macromolecular Chemistry, Worringer Weg 1, 52074 Aachen, Germany.

(1) (a) Welton, T. *Chem. Rev.* **1999**, *99*, 2071. (b) Holbrey, J. D.; Seddon, K. R. *Clean Prod. Processes* **1999**, *1*, 223. (c) Wasserscheid, P.; Keim, W. *Angew. Chem., Int. Ed.* **2000**, *39*, 3772.
(2) (a) Gordon, C. M. *Appl. Catal., A* **2001**, *222*, 101. (b) Sheldon, R. *Chem. Commun.* **2001**, 2399.
(3) Visser, A. E.; Swatlowski, R. P.; Rogers, R. D. *Green Chem.* **2000**, *2*, 1.
(4) Hussey, C. L. In *Chemistry of Nonaqueous Solutions*; Mamantov, G., Popov, A. I., Eds.; VCH: Weinheim, 1994; p 227.
(5) Gordon, C. M.; McLean, A. J. *Chem. Commun.* **2000**, 1395.
(6) (a) Gordon, C. M.; Holbrey, J. D.; Kennedy, A. R.; Seddon, K. R. *J. Mater. Chem.* **1998**, *8*, 2627. (b) Holbrey, J. D.; Seddon, K. R. *J. Chem. Soc., Dalton Trans.* **1999**, 2133. (c) Hardacre, C.; Holbrey, J. D.; McCormac, P. B.; McMath, S. E. J.; Nieuwenhuyzen, M.; Seddon, K. R. *J. Mater. Chem.* **2001**, *11*, 346.
(7) Walden, P. *Bull. Acad. Imper. Sci. (St. Petersburg)* **1914**, 1800.

10.1021/cm021378u CCC: $25.00
Published on Web 07/02/2003

crystalline behavior,[6] but little information was given regarding the structural changes occurring at each phase change. To unravel the nature of the low-temperature process and to collect a detailed characterization of the phase diagram of this material, we have applied a range of strongly complementary techniques to the study of $[C_{16}mim][PF_6]$. Among these techniques is quasi-elastic neutron scattering (QENS) which is a method previously used for dynamical analysis of many different types of materials, including liquid crystals, polymers, and biological membranes. The work reported here is the first example of the use of this technique for the study of ILs. In support of these results, we have also carried out a variable-temperature single-crystal X-ray diffraction study on $[C_{14}mim][PF_6]$. The results of all of these investigations are used to gain important insights into the structure and properties of this family of liquid crystalline salts.

Experimental Section

The salts $[C_{16}mim][PF_6]$ and $[C_{14}mim][PF_6]$ were synthesized as reported previously.[6] The thermal properties of $[C_{16}mim][PF_6]$ were determined by differential scanning calorimetry (DSC) using a Mettler-Toledo DSC 821 differential scanning calorimeter equipped with a TS0801RO sample robot and calibrated using indium and zinc standards. The sample was heated from 223 to 423 K, cooled to 223 K and reheated to 423 K. The heating and cooling rate was 10 K min^{-1}. Phase identification was performed by polarized-light microscopy using an Olympus BH-2 optical microscope equipped with a Linkam THMS 600 heating stage and a TMS 91 control unit.

Impedance data in the range 0.1 Hz to 1 MHz were collected between 253 and 473 K with a Schlumberger-Solartron 1260 impedance analyzer. These data were driven through a IEEE 488 interface by a computer with impedance-gain phase software Z60 version 1.5 from Scribner Associates. The sample was kept at each temperature for at least 20 min before data were collected.

Raman scattering was collected using a Renishaw 2000 microprobe spectrometer (Renishaw Ltd.), with the excitation at 457.6 nm provided by an OmNichrome argon ion laser (Lambda Photometrics). The Renishaw instrument had a notch filter, a single grating, and a cooled charge-coupled device detector. A microscope was used to focus the laser radiation and to collect the 180° Raman scattering. The Ar^+ laser was typically operated at a power of 100 mW. No decomposition of the samples was observed under laser irradiation. Spectra were typically recorded by co-adding 5 or 10 scans of 10 s each, with the grating centered at 2900 and 1100 cm^{-1} for the two main spectral ranges investigated. Low wavenumber spectra were recorded by co-adding five successive continuous scans from 150 to 400 cm^{-1}. In the variable temperature experiments, neat samples were placed between two microscope cover slips and heated using a Linkam PR600 hot stage, which permitted control of the temperature to ±0.1 K. Samples were held isothermally for at least 5 min before recording spectra to ensure that thermal equilibrium had been achieved.

QENS measurements were carried out on the IN16 backscattering spectrometer at the Institut Laue Langevin (ILL), Grenoble, France. Operating at a wavelength $\lambda = 6.271$ Å, this instrument has a 0.9-μeV resolution measured as full width at half peak height and covers the range between $0.40 < Q$ (Å^{-1}) < 1.9. Incoherent elastic neutron scattering data were collected using the fixed-window technique in the temperature range 10−500 K. The sample had a slab geometry with a thickness of 0.2 mm to minimize multiple scattering contributions. Data, once collected, have been normalized to the extrapolation at $T = 0$ K. The contribution of the empty cell has not been subtracted and accounts for a flat contribution, which becomes comparable with the signal from the sample only at the highest temperatures.

Combined SAXS−WAXS measurements were performed on the SAXS beam-line at synchrotron ELETTRA in Trieste, Italy. The X-ray beam was monochromatized by a double crystal Si (1,1,1) and focused on the 2-mm thick samples by a toroidal mirror.[8] The wavelength was 1.54 Å and the beam size was 0.5 × 0.5 mm^2. A sample−detector distance of 1.5 m was used for the SAXS detector. Calibration of the Q-axis was made with wet rat tail tendon for the SAXS region, thus covering a Q range from 0.02 to 0.35 Å^{-1} ($Q = 4\pi/\lambda \sin\theta$, 2θ being the scattering angle). Measurements on $[C_{16}mim][PF_6]$ were carried out over the temperature range 273−333 K at a heating rate of 6 K min^{-1} using a stationary flow of cold N_2 directly onto the sample (Oxford Cryostream Cooler). An electrical heating device was then used to cover the range 303−423 K at the same heating rate. Each reported frame is the average over 10 s accumulation time, thus providing a temperature resolution of approximately 1 K.

Single-crystal X-ray studies were carried out on a Nonius Kappa CCD diffractometer equipped with an Oxford Cryostream variable-temperature device and used Mo Kα radiation ($\lambda = 0.71073$ Å). A tabular, colorless crystal of dimensions 0.50 × 0.18 × 0.12 mm was glued to a glass fiber. A full dataset was recorded at 300 K before collecting short, partial datasets at 10 degree intervals down to 200 K. A gradual but significant increase in the maximum 2θ angle of the observed reflections was apparent. A second full data collection was carried out at 175 K before allowing the sample to warm to 300 K. Both the unit cell obtained and the scattering power of the crystal were similar to those observed at 300 K prior to cooling. Crystallographic and refinement parameters are given below for the 175 K dataset with those for the 300 K dataset given in parentheses where different. For $C_{18}H_{35}F_6N_2P$: found monoclinic, $P2_1/a$, $a = 9.2115(2)$ {9.6823(3)} Å, $b = 9.8729(2)$ {9.5159(2)} Å, $c = 24.2448(5)$ {25.4086(8)} Å, $\beta = 90.509(1)$ {94.215(2)}°, $V = 2204.84(8)$ {2334.7(1)} Å^3, $Z = 4$, $D_c = 1.279$ {1.208} Mg m^{-3}, $\mu = 0.179$ {0.169} mm^{-1}. The structures were solved and refined to convergence on F^2 using programs from the ShelX suite.[9] All non-H atoms were refined anisotropically and all H atoms were placed in calculated positions and in riding modes. Several attempts were made to model the large atomic movements observed at 300 K as disorder over a number of partially occupied sites. As none of these models were stable, and to better facilitate comparison with the 175 K structure, the final solution did not incorporate any disordered components or any geometric constraints or restraints. The resulting model thus incorporates some geometries that are clearly not chemically feasible (especially about C6, C7, and C8) but which are of interest for the purposes of this paper. Final refinement of 4336 {3357}unique data and 246 parameters ($R_{int} = 0.0273$ {0.0633}, $2\theta_{max} = 52.08$ {46.56}°) gave R1 = 0.0400 {0.1096} for 3187 {1403} observed reflections and wR2 = 0.1013 {0.3865} for all reflections. For full details of structural refinement, see Cambridge Data Centre reference numbers CCDC 210033 and 210034.

Results and Discussion

Thermal Behavior. The DSC traces obtained for $[C_{16}mim][PF_6]$ are shown in Figure 1. In each trace, i.e., initial heat, first cool, and subsequent reheat, three phase transitions are evident. On heating, the transition peak temperatures are 290, 348, and 398 K. The latter two transitions were previously assigned as crystalline (C) to smectic A (S_A) and smectic A to isotropic liquid (I), respectively, and the transition temperatures observed are in excellent agreement with those reported by Gordon et al.[6a] On cooling from the isotropic phase,

(8) Amenitsch, H.; Bernstorff, S.; Krieckbaum, M.; Lombardo, D.; Mio, H.; Rappolt, M.; Laggner, P. *J. Appl. Crystallogr.* **1997**, *30*, 87.

(9) Sheldrick, G. M. *SHELXS and SHELXL; Programs for the Solution and Refinement of Crystal Structures*. University of Göttingen: Göttingen, Germany, 1997.

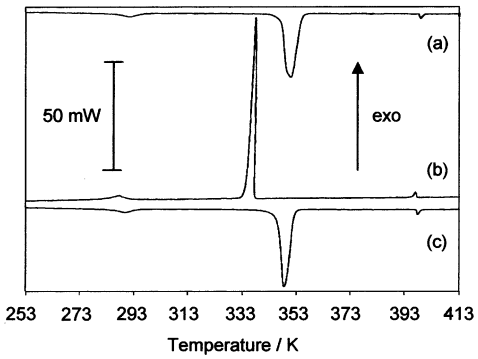

Figure 1. DSC traces observed on (a) heating, (b) cooling, and (c) reheating of $[C_{16}mim][PF_6]$. Heating and cooling rates of 10 °C min^{-1} were employed.

batonnets develop which coalesce to give a focal conic fan texture, supporting the assignment of the phase transition detected at 398 K as S_A-I. At the same time, there is a clear increase in viscosity on formation of the mesophase from the isotropic liquid. On further cooling, the optical texture changes to give a characteristic crystal texture, and thus the transition at 348 K is assigned as $C-S_A$. The low-temperature phase transition at 17 °C is associated with a change in the texture of the crystal phase, suggesting the existence of both low- (C_I) and high-temperature (C_{II}) crystalline polymorphs. This transition has not previously been reported for the $[Rmim][PF_6]$ salts and we will return to a discussion of its assignment later. It should be noted, however, that in salts of the family $[Rmim]_2[PdCl_4]$ (R = C_{10}, C_{12}, C_{14}, C_{16}, and C_{18}) more than one crystalline polymorph was observed at temperatures below the melting point.[6c] In these salts, however, the transition enthalpies were much greater than those observed for C_I-C_{II} in our work, indicating much more dramatic structural changes. The authors suggested that a change from noninterdigitated alkyl chains to interdigitated was occurring; as will be seen later, this is not the case in $[C_{16}mim][PF_6]$.

The entropy change associated with the $C_{II}-S_A$ transition, expressed as the dimensionless quantity $\Delta S/R$, is 12.4 and is in accord with this assignment. By contrast, $\Delta S/R$ for the S_A-I transition is just 0.19 which is surprisingly low for this type of transition. Indeed, such a low value of $\Delta S/R$ would normally be indicative of a nematic−isotropic transition.[10] These values of $\Delta S/R$ are in very good agreement with those published earlier.[6] The value of $\Delta S/R$ associated with the low-temperature transition is 1.44 and thus larger than that associated with the clearing transition, but still much smaller than the values observed by Hardacre et al. for the similar $[PdCl_4]^{2-}$ complexes mentioned above.[6c]

Conductivity. The ionic conductivity of $[C_{16}mim][PF_6]$ is presented in the form of an Arrhenius plot in Figure 2. On heating a large increase in conductivity is observed over the range 338 K ($\sigma = 2 \times 10^{-5}$ S cm^{-1}) to 352 K ($\sigma = 6.3 \times 10^{-4}$ S cm^{-1}). This indicates that this significant change in conductivity is associated with the melting of the sample into the S_A phase (348 K from the DSC measurements). It is interesting to note, however, that the crystal phase C_{II} exhibits appreciable levels of conductivity implying ion mobility in the solid state. On further heating a much smaller step change

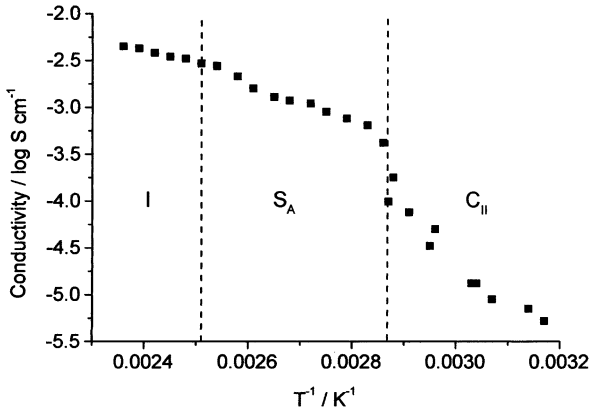

Figure 2. Arrhenius plot of ionic conductivity of $[C_{16}mim][PF_6]$. Dashed lines mark phase changes.

in the conductivity is observed between 100 °C ($\sigma = 2.6 \times 10^{-3}$ S cm^{-1}) and 120 °C ($\sigma = 2.5 \times 10^{-3}$ S cm^{-1}) and which is associated with the S_A-I transition. On cooling to lower temperatures (<298 K) the conductivity falls rapidly to ca. 10^{-8} S cm^{-1}, a level at which the instrument used for these measurements cannot give accurate data. This change is therefore not shown in Figure 2.

The small change in the ionic conductivity accompanying the S_A-I transition implies that the ionic environment changes little at this transition. Thus, large ionic aggregates must persist into the isotropic phase, and the volume change is likely to be small over this transition. The change in the orientational and translational order at the clearing point would not, therefore, be as large as expected, which may account for the low value of $\Delta S(S_A-I)/R$. A similar explanation has been recently suggested to rationalize the low values of $\Delta S(S_A-I)/R$ generally observed for carbohydrate-based liquid crystals for which hydrogen-bonded aggregates are proposed to exist in the isotropic phase.[11] It should also be noted that in the S_A phase exhibited by $[C_{16}mim][PF_6]$ the anions are disordered, which will also reduce $\Delta S(S_A-I)/R$. The small decrease in conductivity observed on cooling the isotropic phase into the S_A phase may reflect the multidomain structure of the latter phase. The equivalent of grain boundaries existing between these domains will reduce the conductivity. This implies that an aligned sample should exhibit a higher conductivity and this now needs to be investigated. Similarly small changes in conductivity have been observed at the clearing transition of liquid crystal polymer electrolytes.[12] It should also be noted that a recent paper reports the conductivity of $[C_{18}mim][BF_4]$ and its mixtures with $[C_4mim][BF_4]$.[13] Conductivity values reported for the crystalline and smectic A phases of polydomain samples were comparatively similar to those obtained for $[C_{16}mim][PF_6]$. Importantly, however, the conductivity of aligned samples was found to be considerably higher.

The large increase in the conductivity at the melting point (T = 348 K) reflects a marked increase in ion mobility although the conductivity measured below the melting point is surprisingly high. It is important to note that in the solid phases the conductivity is presumed

(10) Imrie, C. T.; Taylor, L. *Liq. Cryst.* **1989**, *6*, 1.
(11) Cook, A. G.; Wardell, J. L.; Imrie, C. T. *Liq. Cryst.* submitted for publication.

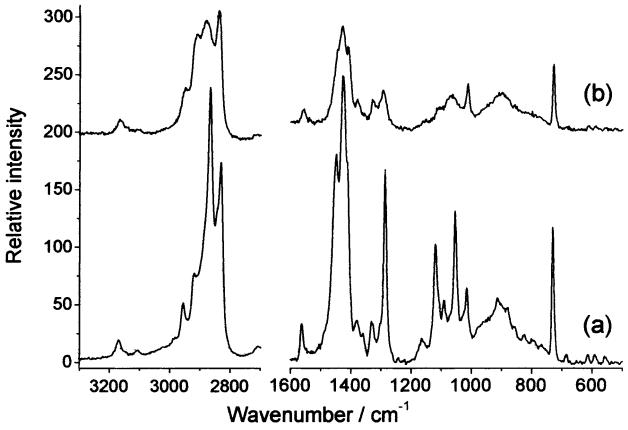

Figure 3. Raman spectra of $[C_{16}mim][PF_6]$ recorded at (a) 298 K and (b) 353 K.

to be anionic as the cations are immobilized. A dramatic decrease in conductivity (to levels below those measurable by our equipment) is associated with formation of the lower-temperature crystalline phase. This strongly suggests that in the C_{II} phase there must be the possibility of ionic motion, presumably of the anions as these are much smaller than the cations. The decoupling of localized molecular motion from viscous flow allows for ionic mobility via a rotator mechanism in the solid state. Ionic conductivity has been observed previously in plastic crystals.[14] At the melting, or $C_{II}-S_A$, phase transition the increase in free volume provides for higher ionic mobility and possibly cooperative motion of the ions.

Raman Spectroscopy. Raman spectroscopy was found to be a very convenient technique to obtain structural information on these salts. The vibrational spectra of long-alkyl-chain-substituted $[Rmim]^+$ salts of this type have not been reported before, although the infrared spectra of ionic liquids containing shorter alkyl chains have been discussed in some detail.[15] Using a microscope hot stage in combination with a Raman microscope it was possible to record spectra over most of the temperature range required. Very distinct differences were observed between the C_{II} and S_A phases as might be expected. The lowest temperature at which Raman spectra could be recorded was 263 K, at which point the sample would be expected to be in the C_I phase. The spectra at this temperature were little different from those recorded at 298 K, suggesting that this technique is insufficiently sensitive to distinguish the C_I and C_{II} phases. The only notable difference was a reduction in overall signal intensity at the lower temperature, but this may simply arise from greater light scattering caused by condensation at temperatures below freezing. Figure 3 shows Raman spectra recorded at 298 and 353 K. Peaks in the region 2700−3300 cm^{-1} arise from ν(CH) modes, whereas those in the region 500−1600 cm^{-1} arise principally from a combination of ν(CC) and cation bending modes, as well as the intense $\nu(PF_6)_s$ mode at 732 cm^{-1}.

The most distinct changes are observed in the ν(CH) region. At low temperatures the spectrum is dominated by the symmetric and antisymmetric CH_2 stretching modes ($\nu(CH_2)_s$ and $\nu(CH_2)_{as}$) at 2830 and 2866 cm^{-1}, respectively. The ratio, r, of peak heights of these bands ($\nu(CH)_s/\nu(CH)_{as}$) has been used as a measure of the degree of order in crystalline alkanes, fatty acids, and their esters,[16] and long alkyl chain containing salts.[17] Although caution must be taken when considering different classes of material and in comparison of different phases, in examples of related crystalline salts reported to date it has been shown that a lower value of r indicates a larger degree of linearity. For $[C_{16}mim][PF_6]$, $r = 0.73$, compared with values of 0.46 in $[C_{10}H_{21}NH_3]Cl$ and 0.60 in $[C_{10}H_{21}NH_3]_2[CdCl_4]$.[17] It has previously been shown that the crystal structure of $[C_{12}mim][PF_6]$ shows a "kinked" alkyl chain,[6] and a similar structure is observed for $[C_{14}mim][PF_6]$, as will be reported below. Assuming that $[C_{16}mim][PF_6]$ has a similar structure, as is suggested by the similarity in the powder X-ray diffraction patterns, nonlinearity in the alkyl chain may account for the relatively high value of r. On passing through the $C_{II}-S_A$ phase transition, distinct changes are observed in the ν(CH) region. Most notably, the band at 2866 cm^{-1} disappears, to be replaced with a broader peak centered at ca. 2880 cm^{-1}. This type of profile is almost identical to that observed for $[C_{16}py]Cl$ in aqueous solution over the same region.[18]

Over the same phase change, the bands in the 500−1600 cm^{-1} region show a decrease in overall intensity, and the spectrum becomes more simple. There is little change in the position of the $\nu(PF_6)_{as}$ band (from 732 cm^{-1} at 298 K to 727 cm^{-1} at 353 K), suggesting little change in the geometry of the anion on formation of the S_A phase. The relatively intense bands at 1119 and 1055 cm^{-1} can be assigned as $\nu(CC)_s$ and $\nu(CC)_{as}$ respectively, and are reported to be indicative of the presence of all-trans methylene units.[19] The very large decrease in intensity of these bands, accompanied by the appearance of a broad band at ca. 1065 cm^{-1} can be assigned to the appearance of gauche conformers at the expense of the all-trans form.[20] All of these data clearly suggest that conformational melting of the alkyl chains has occurred on formation of the mesophase. Furthermore, the relatively small changes observed in the anion band on formation of the mesophase supports its assignment as a smectic phase as the overall layer structure (presumably largely controlled by the anions and the cationic headgroup) must be retained (see also the discussion of SAXS data for a confirmation of this interpretation). The spectrum of the S_A phase remained unchanged up to the S_A-I transition at 398 K, at which point the intensity of the spectrum decreased markedly. Cooling the sample to reform the S_A and crystalline

(12) (a) McHattie, G. S.; Imrie, C. T.; Ingram, M. D. *Electrochim. Acta* **1998**, *43*, 1151. (b) Imrie, C. T.; Ingram, M. D.; McHattie, G. S. *J. Phys. Chem.* **1999**, *103*, 4132. (c) Imrie, C. T.; Ingram, M. D.; McHattie, G. S. *Adv. Mater.* **1999**, *11*, 832.
(13) Yoshio, M.; Mukai, T.; Kanie, K.; Yoshizawa, M.; Ohno, H.; Kato, T. *Chem. Lett.* **2002**, 320.
(14) MacFarlane, D. R.; Forsyth, M. *Adv. Mater.* **2001**, *13*, 957.
(15) (a) Tait, S.; Osteryoung, R. *Inorg. Chem.* **1984**, *23*, 4352. (b) Dieter, K. M.; Dymek, C. J., Jr.; Heimer, N. E.; Rovang, J. W.; Wilkes, J. S. *J. Am. Chem. Soc.* **1988**, *110*, 2722.
(16) Snyder, R. G.; Hsu, S. L.; Krimm, S. *Spectrochim. Acta* **1978**, *34A*, 395.
(17) Casal, H. L.; Cameron, D. G.; Mantsch, H. H. *J. Phys. Chem.* **1985**, *89*, 5557.
(18) Sun, S.; Birke, R. L.; Lombardi, J. R.; *J. Phys. Chem.* **1990**, *94*, 2005.
(19) Ishioka, T. *Bull. Chem. Soc. Jpn.* **1991**, *64*, 2174.
(20) Huang, C.; Levin, I. W. *J. Phys. Chem.* **1983**, *87*, 1509.

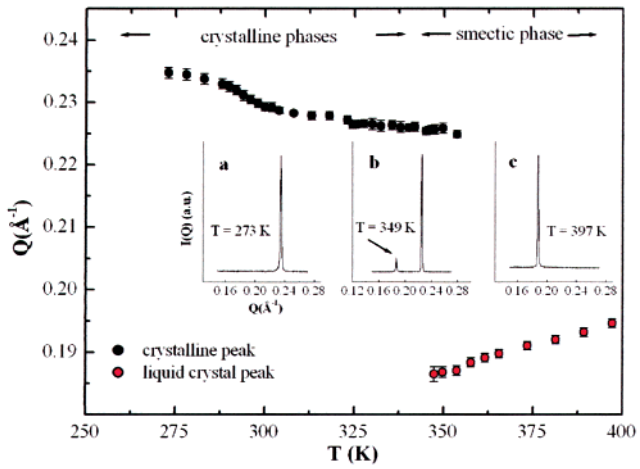

Figure 4. Temperature dependence of the SAXS peaks from [C_{16}mim][PF_6]; the points refer to the peak positions and the error bars refer to their fwhm. In the insets, representative SAXS patterns are reported as a function of Q at selected temperatures.

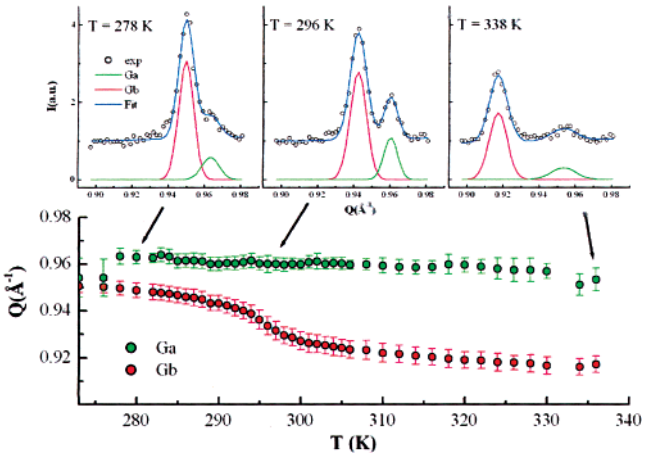

Figure 5. Temperature dependence of selected WAXS peaks from [C_{16}mim][PF_6]; the points refer to the peak positions and the error bars refer to their fwhm.

phases gave spectra effectively identical to those shown in Figure 3(b) and 3(a), respectively, indicating that the same structures were formed on cooling as on heating.

X-ray and Neutron Investigations. *S-WAXS.* Figures 4 and 5 show the temperature dependence of the small- and wide-angle X-ray scattering (S-WAXS) of [C_{16}mim][PF_6] over the temperature range 273−423 K. Upon melting of the crystalline phase to form the mesophase (indicated by the drastic change of the SAXS pattern at ca. 348 K), the WAXS pattern changes from a multiplicity of peaks to an amorphous halo. This indicates a loss of the short range order. On the basis of polarizing optical microscopy results, where homeotropic domains had been observed as well as focal conic textures, we had previously assigned the mesophase as S_A.[6a] The S-WAXS data reported here are consistent with this assignment. In the SAXS data, a single peak is observed whose position varies depending on the temperature. A distinct shift in the position of the peak is observed at each of the phase transitions, as can be seen in Figure 4. This peak has been associated with the existence of layered structures in both the crystalline and S_A phases. The linear dependence of the layer spacing on the alkyl chain length (data not shown) strongly suggests that this corresponds to the distance between layers of interdigitating molecules (henceforth referred to as *d*-spacing). The sharp peak in the SAXS region disappears rapidly at 398 K, as would be expected on formation of an isotropic liquid. Close examination of the SAXS region at higher temperatures, however, indicates that a weak broad peak remains at the same position. This suggests that a small amount of residual short range order remains in the system even above the clearing point.

It can be seen that that the positions of the SAXS peaks associated with the C_{II} and S_A phases show differing temperature dependence. In the C_{II} phase the *d*-spacing increases with temperature, whereas the S_A phase shows the opposite behavior. Moreover, the S_A *d*-spacing is always *longer* than that for C_{II}. Such behavior has recently been noted for similar ILs,[21] and has been rationalized in the following manner. It has been suggested that in the S_A phase the alkyl chains remain interdigitated, like they are in the C_{II} phase, but are disordered. The Raman spectral data reported above support this conclusion. In the C_{II} phase the spacing is generally $l < d < 2l$, where l is the fully extended alkyl chain length. This implies that the alkyl chains are either interdigitated or at an angle to the unit cell planes (or both), a conclusion that is supported by the crystal structure of [C_{12}mim][PF_6].[6] The observation of an increased spacing on formation of the S_A phase can be rationalized by assuming that, as a consequence of disordering of the alkyl chain (also indicated by the disappearance of the WAXS peaks upon transition from C_{II} to S_A and by Raman data), a decrease of the tilting angle occurs. Alternatively, it can be considered that in the S_A phase the alkyl chains are characterized by a higher degree of disorder which leads to a stronger repulsion (due to steric effects) between the interdigitated layers. It is possible that these two effects take place simultaneously. Whatever the explanation, the very narrow shape of the SAXS peaks for both C_{II} and S_A phases indicates that the distribution of spacing between neighbor layers is monodispersed, and furthermore that the melting process occurring upon transition from C_{II} to S_A does not substantially affect such monodispersity. On the other hand, on a local level, the transition induces a substantial loss of short range order, as indicated by the temperature dependence of the WAXS pattern.

A change in the SAXS−WAXS patterns can also be seen at the transition $C_I \rightarrow C_{II}$ ($T \sim 288$ K), with a shift in the position of the SAXS peak indicating a marked increase in the layer spacing as the temperature is increased. This information can be of relevance in trying to understand the nature of this thermal transition, which turns out to be associated to structural changes at both short and long spatial scales (as illustrated by the corresponding changes in the WAXS spectra).

The WAXS profiles can also be fruitfully used to extract important information on the nature of the phase diagram of [C_{16}mim][PF_6]. These data indicate that the short range order is affected by the thermal events occurring at 290 and 348 K. Most notably, in the region around 343−348 K the WAXS peaks progres-

(21) Bradley, A. E.; Hardacre, C.; Holbrey, J. D.; Johnston, S.; McMath, S. E. J.; Nieuwenhuyzen, M. *Chem. Mater.* **2002**, *14*, 629.

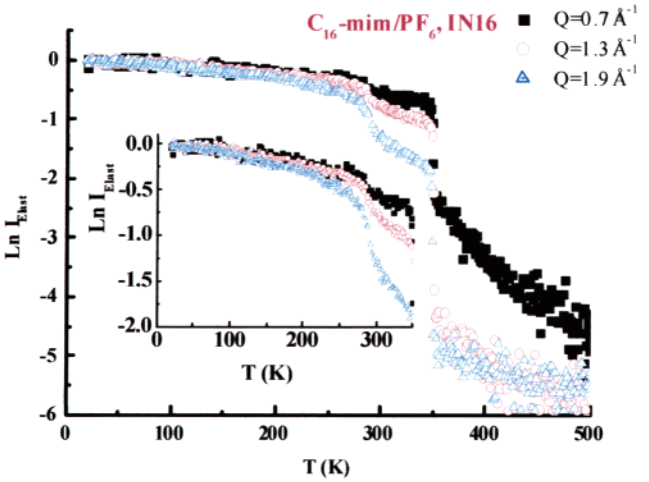

Figure 6. Temperature dependence of the elastically scattered intensity from [C_{16}mim][PF_6], as collected at three different Q values: 0.70, 1.30, and 1.90 Å^{-1}. In the inset, the same data are zoomed in the low-temperature region.

sively disappear as a consequence of the $C_{II}-S_A$ transition. This suggests an almost complete loss of short range order on formation of the S_A phase. Figure 5 shows a small extract of the WAXS data recorded over the temperature range 273−336 K. With regard to the lower temperature transition, over a wide temperature range from 283 to 303 K, the positions of some of the WAXS peaks change drastically, although continuously, across the C_I-C_{II} transition. This evidence indicates that a substantial degree of both short and long range order is preserved over the low-temperature transition, while the high-temperature transition involves a drastic loss of correlation at short distances, but that the long range order is maintained.

Quasi-Elastic Neutron Scattering. The results presented up to here mainly refer to thermodynamic and structural characterization of [C_{16}mim][PF_6]. We now report on the first quasi-elastic neutron scattering (QENS) results recorded for this type of salt. This kind of experiment provides information on the dynamic events occurring in the material. In particular, as neutrons are particularly sensitive to hydrogen atoms, QENS data can be used to unravel the dynamics of the alkyl chains of [C_{16}mim][PF_6], as 33 out of the 39 hydrogen atoms in the molecule (i.e., ∼85%) belong to the alkyl chain. In Figure 6 we report the logarithm of the elastically scattered intensity (ESI), ln I_{EL}, as a function of temperature. This is obtained using a high-resolution backscattering spectrometer, which measures the number of neutrons elastically scattered by the sample: at each temperature the number of neutrons whose energy did not change within the instrumental resolution, (in this case 0.9 μeV) is reported. As soon as the temperature is high enough to activate a dynamic process, this will couple with the incoming neutron beam and an energy exchange will occur between the sample and the neutrons, the exchange being related to the amount of energy necessary to promote the dynamic process.

In Figure 6, three curves are shown for different values of the momentum transfer Q. The Q dependence is one of the most important features of neutron scattering as compared to other spectroscopic techniques such as dielectric or mechanical spectroscopies, as it allows derivation of information on the spatial extent of the relaxation process on a size comparable with atomic/molecular processes ($r \sim 5$ Å). A number of interesting features can be derived from the plots in Figure 6. In the inset, where the low-temperature portion is expanded, it can be seen that there is a linear dependence of ln I_{EL} on temperature over the temperature range 10−120 K. This behavior is generally attributed to the Lamb−Mössbauer factor, which refers to the exchange of energy between matter and neutrons due to the oscillations of atoms around their equilibrium position. In this case, no relevant dynamic processes occur between 0 and 120 K. Above this threshold temperature, a change in slope of ln I_{EL} is observed. This kind of behavior can be explained on the basis of similar observations made in polymer glasses containing short alkyl groups. At temperatures above 100 K rotation of methyl groups occurs, a dynamic process that can exchange energy with neutrons. A similar exchange of energy can also occur between longer alkyl chains and neutrons and thus lead to a decrease of the ESI. The geometrical nature of the alkyl chain relaxation implies that the decrease in ESI will have a Q dependence that can be rationalized in terms of a spatial model. The fact that a methyl group and a longer (C_{16}) alkyl chain coexist in our sample complicates the scenario, as relaxation of the different units will be superimposed. We are presently pursuing the synthesis of a selectively deuterated sample in order to separate the contribution of the methyl and hexadecyl groups. At the highest Q reported ($Q = 1.90$ Å^{-1}), where the decrease in ESI is most sensitive, it can be observed that at 200 K a further change in slope occurs. It is possible that this weak signal is a fingerprint of a glass transition as seen by neutrons. As this material is crystalline, it is very difficult to characterize the glass transition by conventional techniques (such as DSC), as the amorphous portion of the sample (which relaxes upon transition from glassy to rubbery material) is very small and also constrained by the surrounding crystalline portion. It has been noted recently that in a similar class of materials, [$C_n$mim][BF_4], the samples containing an alkyl chain of 4−9 carbon atoms display glass transition temperatures of approximately 195 K.[6b] A more drastic decay in the ESI is found in the range 280−290 K; this corresponds to the C_I-C_{II} transition, as seen in the DSC, conductivity, and SAXS/WAXS results. After such a transition, a considerable amount of motion can be detected as indicated by the steeper slope of the ESI in the range 280 K < T < 350 K. This is evidence of increased flexibility in the alkyl chain, which can exchange energy with the incoming neutron beam in this temperature range. At 345 K a further, very large, decrease in ESI is found, corresponding to the $C_{II}-S_A$ transition. Such a large decrease is caused by the complete conformational melting of the crystalline environment, as indicated by the Raman spectra. As a consequence, the chains are now relatively free to move and exchange energy with the neutrons. Because of the high level of noise it was not possible to identify reliably the final transition from S_A to I.

We assume that the temperature dependence of the ESI follows the Lamb−Mössbauer law:

$$\mathrm{ESI} = \exp(-1/3\, Q^2\langle u(T)^2\rangle)$$

where $\langle u(T)^2\rangle$ is the mean square displacement (MSD) of the scatterer (in our case the H atoms) at temperature T.[22] In a plot of ln ESI vs Q^2, the slope of the linear interpolation of these data provides an estimate of $\langle u(T)^2\rangle$. Accordingly, in Figure 7, the MSD for $[C_{16}mim][PF_6]$ is plotted as a function of temperature. The complex behavior observed in Figure 6 is confirmed by the data plotted in Figure 7. However, the MSD is more directly related to a tangible physical quantity such as the displacement of the H atoms from their equilibrium positions and so it is a measure of the mobility of such atoms in the material. In Figure 7, we highlight all the different temperature regimes that characterize the dynamics of $[C_{16}mim][PF_6]$. Thus, it can be seen that the degree of displacement is relatively low below the C_I-C_{II} transition. The large increase in $\langle u^2\rangle$ at this temperature supports the suggestion that this transition is accompanied by a large increase in the freedom of the alkyl chain.

In an attempt to further explore the nature of the polymorphism of $[C_{16}mim][PF_6]$, and in particular to understand the nature of the low-temperature thermal transition C_I-C_{II}, we decided to compare directly the temperature dependence of a number of reported quantities in the temperature range across this transition. In Figure 8, a comparison between the ln ESI (derived with the QENS technique and providing information on the mobility of H atoms), the crystalline SAXS peak position (providing information on the characteristic long range spacing), and one selected WAXS peak position (providing information on the short range order) is shown as a function of temperature. No horizontal arbitrary shift has been applied to the data and only a vertical shift, accounting for the fact that completely different quantities are compared, has been applied. It can be seen clearly that the three different techniques have similar behavior across the C_I-C_{II} transition. This result is rather unexpected: although we stress that we are comparing distances and mobility, still the results we are presenting seem to indicate that the thermal transition C_I-C_{II} is associated with a substantial increase in the mobility of H atoms, which has a striking counterpart both at short ($r \sim 3-5$ Å) and long ($r \sim 30$ Å) range.

Single-Crystal Investigations of $[C_{14}mim][PF_6]$. Direct investigations of the low-temperature phase transition of $[C_{16}mim][PF_6]$ could be assisted by the application of variable-temperature single-crystal X-ray diffraction studies. Unfortunately it proved impossible to grow crystals of this species of sufficient quality. Suitable crystals were obtained for the analogous salt $[C_{14}mim][PF_6]$, however. DSC and S-WAXS measurements showed that the thermal behavior of the two salts were exactly analogous, although the transition temperatures were lower for the C_I-C_{II}, $C_{II}-S_A$, and S_A-I transitions in the C_{14} analogue (ca. 278, 347, and 350 K, respectively) (data not shown, manuscript in preparation). Structures were recorded over a range of temperatures from 175 to 300 K, and those recorded at 175 and 300 K are illustrated in Figure 9.

(22) Frick, B.; Fetters, L. J. *Macromolecules* **1994**, *27*, 974.

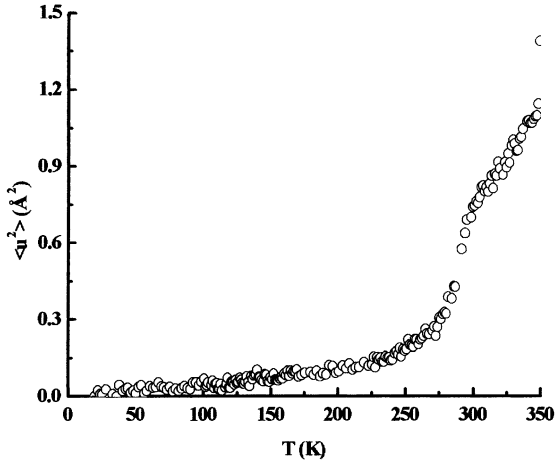

Figure 7. Temperature dependence of the mean square displacement as obtained from the Q dependence of the data reported in Figure 6.

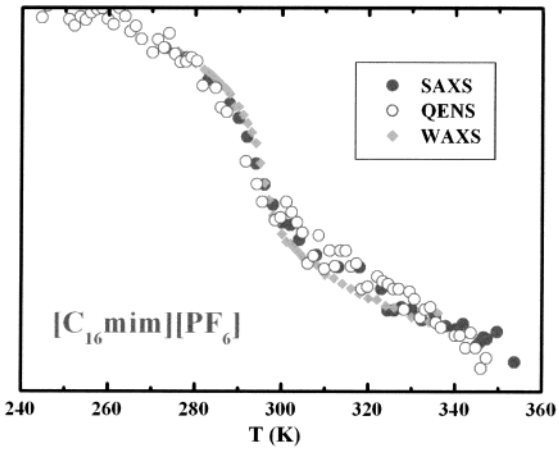

Figure 8. Comparison of the temperature dependence of ln I_{EL} (data from Figure 6), of the SAXS peak position and of a selected WAXS peak position. Data have been vertically shifted so as to give a direct comparison of their temperature dependence, although units are not included on this axis as three different quantities are being measured.

The low-temperature structure is well ordered and shows only localized thermal displacements as would be expected in the terminal methyl groups and the $[PF_6]^-$ anion. Overall, the structure is extremely similar to the analogous structure of $[C_{12}mim][PF_6]$ reported previously,[6] with a clearly defined arrangement of interdigitated alkyl chains separating rows of imidazolium headgroups and anions. The alkyl chain extends fully in an eclipsed geometry from C7 to C18 but is distorted between C7 and the aryl ring to form a "crank-handle"-like arrangement. It is clear from Figure 9(b) that there is considerably more atomic motion throughout both the cation and anion at 300 K than there is at 175 K. Overall, however, the basic structures are approximately the same, suggesting that the phase transition C_I-C_{II} does not involve a major structural change, but is largely marked by an increase in the degree of motion in the anion and the alkyl chain. The increase in motion, however, is not uniform and is most exaggerated at C6, C7, and C8 in the region of the "crank-handle" and also in the anion and toward the end of the alkyl chain. As noted in the Experimental Section these movements are so extreme that a highly disor-

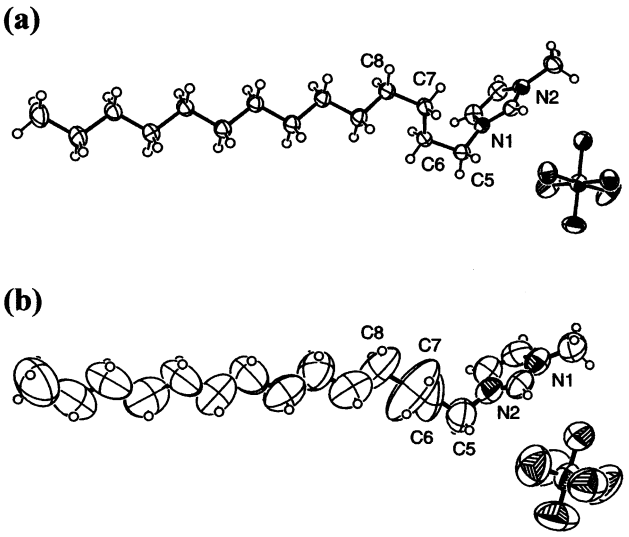

Figure 9. Crystal structure of $[C_{14}mim][PF_6]$ recorded at (a) 175 K and (b) 300 K. The atomic positions are represented by 50% ellipsoids.

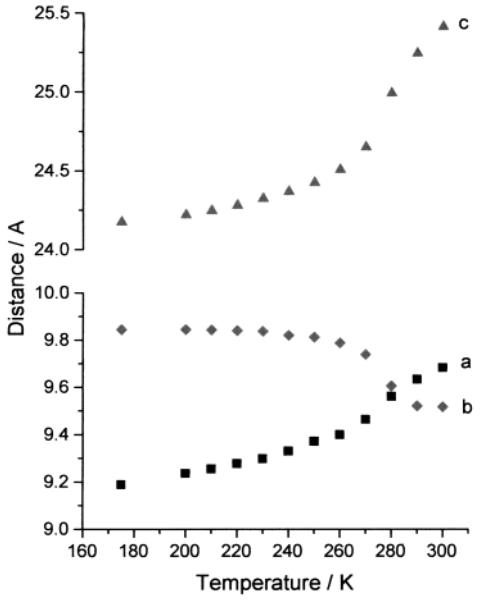

Figure 10. Unit cell dimensions *a*, *b*, and *c* of $[C_{14}mim][PF_6]$ recorded at a range of different temperatures between 175 and 300 K.

dered model is probably most appropriate especially for the C6−C8 region and the $[PF_6]^-$ anion, and possibly also for the remainder of the alkyl chain. Only the atoms of the aryl ring can be placed with any certainty.

Despite the obvious unreliability of the 300 K structure it does support the evidence from the other techniques. The increased anionic freedom at higher temperatures may explain the great increase in conductivity between the lower and higher temperatures. Furthermore, the great increase in freedom of the alkyl chains exactly mirrors the QENS results. The variation in unit cell dimensions *a*, *b*, and *c* with temperature is illustrated in Figure 10. The C_I-C_{II} phase transition can clearly be seen at ca. 270 K, marked by a large increase in *c* (equivalent to the *d*-spacing identified from the SAXS results reported above) and a smaller increase in *a*. Curiously, the other dimension *b* decreases in size on passing through this phase transition. The overall volume of the unit cell increases with increasing temperature, however, with a clear discontinuity at the transition temperature indicating the existence of two distinct polymorphic forms.

Conclusions

We have used a number of complementary techniques to analyze the structures of three different phases of $[C_{16}mim][PF_6]$ and $[C_{14}mim][PF_6]$. For the first time in ionic liquid crystals of this type, a range of thermal, spectroscopic, scattering, and diffraction techniques has been employed to allow a detailed analysis of the behavior of each phase. Furthermore, our results have demonstrated the existence of a hitherto unidentified solid-phase transition C_I-C_{II}. The data reported above allow the most detailed discussion to date of the structural nature of the C_I-C_{II} and $C_{II}-S_A$ transitions in salts of this type, and also of the nature of each phase. Considering the former transition, we propose that it involves complex structural rearrangements driven by a thermally activated increase of the mobility. The strong QENS signal suggests that increased motion of the alkyl chains is principally responsible for the observed phenomenon. The conductivity results, however, indicate that the transition also involves an increase in anion mobility (as the imidazolium headgroups would be expected to remain frozen in a crystalline structure). This implies that the triggering of motion in the alkyl chains also allows the anions to escape from the frozen configuration in the C_{II} phase, thus greatly increasing conductivity. This conclusion is supported by the results gained from the single-crystal diffraction studies on the C_{14} analogue, where the smallest degree of disorder was observed in the cationic headgroup, while considerable motion was observed in the alkyl chain and the anion. Finally, the conductivity is surprisingly high in the C_{II} phase for a crystalline sample, suggesting that salts of this type might display useful applications as conducting materials even in the solid state.

With regard to the $C_{II}-S_A$ transition, the QENS, S-WAXS, and Raman data show that complete conformational melting occurs in the alkyl chain region on formation of the mesophase. At the same time, sufficient order must remain in the cation/anion region to sustain the interdigitated S_A structure with an extremely monodispersed layer spacing. The considerable increase in conductivity over the $C_{II}-S_A$ transition also suggests that there is considerably greater anionic freedom in the S_A phase than in C_{II}. These results are supported by the relatively large entropy change for the transition measured using DSC.

In light of these results, it is perhaps surprising that such good monodispersion is observed right up to the melting point. The layer spacing in the S_A phase decreases as the temperature is increased, but the QENS results suggest an ever-increasing degree of freedom for the alkyl chains. All of the data also indicate that relatively little structural change occurs on formation of the isotropic liquid phase. The entropy change for the transition was lower than expected for an S_A mesophase, but this was echoed by the relatively small increase in conductivity. It is perhaps not surprising that it proved impossible to identify the S_A-I transition in the QENS

measurements given that this is a measure of the motion of the hydrogen atoms, most of which are already free to move at the clearing point. In fact, the only major changes over the S_A-I transition were observed in the SAXS measurements indicating loss of the layer structure. As noted previously, however, a small residual peak above the clearing point suggested that some aggregation is retained even in the isotropic phase.

In this paper we have shown that a range of different techniques may be applied in a complementary manner to assist in the understanding of the phase diagram of ILs and their crystalline analogues. In particular, it appears that scattering techniques such as QENS might provide valuable information regarding the nature of these materials over a wide temperature range. Such information will be very valuable in helping to understand the properties of these materials. We propose to continue these investigations with a larger range of related salts with different anions or cations to ascertain whether the structural changes seen here are universal.

Acknowledgment. We gratefully thank the instrument representatives of IN16 (T. Seydel, ILL) and SAXS (H. Amenitsch and S. Bernstorff, Elettra) for their assistance. ILL and European Community (Human Potential Program Transnational Access to Major Research Infrastructures EU Contract HPRI-CT-1999-00033) are acknowledged for financial support for the QENS and S-WAXS experiments, respectively. C.M.G. thanks the Royal Society for the award of an equipment grant and the Royal Society of Edinburgh for the award of a BP Research Fellowship. Mrs. V. Baiata (University of Palermo, Italy) is also acknowledged for help with data analysis.

Supporting Information Available: Complete listing of the optimized geometries and other data for $[C_{14}mim][PF_6]$ at 175 and 298 K (CIF). This material is available free of charge via the Internet at http://pubs.acs.org.

CM021378U